Article

Defect Characterization Using Raw Admittance Spectroscopy

Jian V. Li*

Read Online
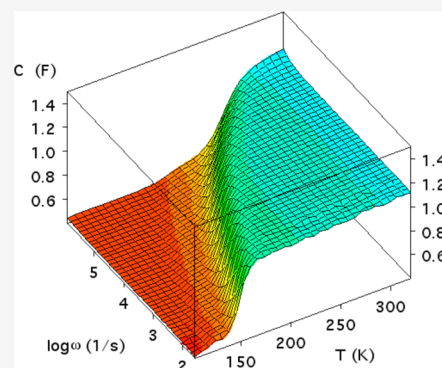
ACCESS | Metrics & More | Article Recommendations | Supporting Information

ABSTRACT: We report a characterization technique that offers substantial improvement over the conventional practice of admittance spectroscopy, specifically in the processing of the admittance signal and the extraction of activation energy E_a and the attempt-to-escape frequency ν_0, of the thermal activated process responsible for the admittance signal, most commonly being from electrically active defects in semiconductor materials. The extraction of these two parameters traditionally follows the procedure of conducting frequency or temperature differentiation of the raw admittance, identifying positions of the defect-signature peak, constructing an Arrhenius plot using the peak positions, and extracting E_a and ν_0 by line fitting. We present a suite of Arrhenius transformations to transform and match the isorate and isothermal scans, carried out at a fixed point of the two-dimensional temperature−rate experimental space, onto one of the four virtual spaces: activation energy, the attempt-to-escape frequency, temperature, and rate. We match the Arrhenius-transformed scans to each other to extract E_a and ν_0 using only the raw capacitance and conductance data without taking the frequency/temperature derivative or using the Arrhenius plot.

INTRODUCTION

Admittance spectroscopy[1] has been extensively[2] used to detect electrically active defects in semiconductor materials and characterize their properties: concentrations, energetic locations, and carrier capture cross sections. Essentially, admittance spectroscopy[3] collects the small-signal charge response of a carrier-defect interactive system present in a semiconductor junction whose bias is modulated at a variable frequency. The signature[4] of a defect is the observation of a transition of the complex admittance signal at a certain frequency and temperature. The magnitude of this capacitance transition can be used to determine the defect density. The frequency and temperature of the transition are dictated by the emission/capture rate of carriers, which is described by[5]

$$\nu = \nu_0 \exp(-E_a/k_B T) \qquad (1)$$

where ν is the emission rate of carriers from a defect located at an energetic distance of E_a away from one of the carrier conduction band edges, ν_0 is the attempt-to-escape frequency, which also contains information regarding the carrier capture cross section, k_B is Boltzmann's constant, and T is the temperature. The symbol E_a stands for activation energy, implying that the Shockleyf−Read−Hall emission/capture of carriers from/to a defect is a thermally activated process[5] and that eq 1 is essentially the Arrhenius equation.[6] Admittance spectroscopy has been applied to investigations of other thermally activated processes in physical and chemical sciences such as band offset in a superlattice.[7]

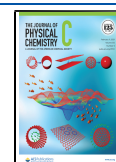Accurate and effective measurement of the activation energy E_a and the attempt-to-escape frequency ν_0 is vital to understand the defects and other thermally activated processes being investigated by admittance spectroscopy. To date, E_a and ν_0 have been extracted almost exclusively using the standard Arrhenius plot line fitting (APL) method.[1] At the measurement temperature, the common practice is to take the derivative of the frequency-dependent capacitance spectrum $C(f)$ with respect to the logarithmic frequency to obtain the frequency derivative[1] capacitance spectrum $f dC/df$ or the temperature derivative[8] dC/dT. A peak appears in the frequency derivative capacitance spectrum at the demarcation frequency[1] where the defect-induced capacitance transition occurs.[9] The peak frequency, which varies with temperature, is recorded at a series of temperature points. One then plots the semilogarithmic plot of peak frequency versus inverse temperature, i.e., an Arrhenius plot of $\ln(\nu)$ versus T^{-1}. Finally, line fitting is performed to the Arrhenius plot data to extract E_a and ν_0 from the slope and intercept, respectively, according to eq 1. Note that we indistinguishably use the terms rate ν, frequency f, and angular frequency ω in this work without arousing ambiguity.

The operation of numerically taking the frequency derivative usually deteriorates the signal-to-noise ratio. Consequently, identification of the exact peak position in the frequency differentiated capacitance spectrum is not always accurate and

may require curve fitting of the entire peak. In practice, the Arrhenius plot line fitting method requires more than a few peak data, collected over a sufficiently wide window of temperature/rate, to yield high-quality extraction of E_a and ν_0.[10] Attempts to increase the number of Arrhenius plot data points and the range of scanned frequencies and temperatures demand more sophisticated and costly electronic and cryogenic apparatus. The above critique of the classical APL method reveals room for improvement and innovation in admittance spectroscopy analysis.[11] Notably, it is desirable to extract E_a and ν_0 without taking the capacitance derivative against either temperature or frequency, having to fit the derivative capacitance spectrum to reliably identify the peak position, or using merely a subset of one-dimensional data such as $\nu(T)$.

In this work, we develop the Arrhenius transformation and matching (ATM) method, which is based on the fundamental temperature–rate duality relationship and capable of extracting E_a and ν_0 from the admittance spectroscopy data in the entire two-dimensional temperature–rate plane without using the Arrhenius plot, using the raw admittance data without taking the capacitance derivative against either temperature or frequency.

EXPERIMENTAL SECTION

We used an impedance analyzer (4294A from Agilent Technologies, now Keysight) to collect the admittance data. A GaAsN solar cell sample, MF166, also investigated in ref 12 by Johnston and Kurtz, was used to demonstrate the method developed in this work. Briefly, the device area for the GaAsN solar cell is 1×1 cm^2. The device is a PN junction grown by the MBE method. The GaAsN composition is 1.2% with a bandgap of 1.2 eV. The carrier concentration on the P side, indicated by capacitance–voltage measurement at 100 kHz and 300 K, is 1.38×10^{17} cm^{-3}. This solar cell device was known to contain defects that are electrically active.[12] Obviously, any other Schottky or PN junction with a suitable defect for observation would serve the purpose of this work, which is experimental technique development.

One calibrated silicon diode-type temperature sensor (Lakeshore DT-670) was embedded inside an oxygen-free beryllium copper sample stage attached to the cold head of a closed-cycle He-cooled cryostat (Janis model M-22). Two 25-ohm resistive-type cartridge heaters were inserted between the cold head of the cryostat and the sample stage to provide a means of heating the latter. The temperature of the sample stage was stabilized at any setting temperature between 12 and 450 K, to within 0.01 K, through a proportional-integral-derivative control algorithm optimized for the above thermal system. A second calibrated silicon diode-type temperature sensor (Lakeshore DT-670) was mechanically clamped directly on top of the sample to ensure best thermal contact to the sample and temperature measurement thereof.

The 4294A impedance analyzer was configured to scan over the frequency range of 100 Hz to 1 MHz. The GaAsN sample was subject to zero DC bias voltage, while a root-mean-square value of 35 mV was used for the AC modulation voltage. Typical frequency derivative capacitance spectra, processed from the raw capacitance versus frequency spectra, are shown in Figure 1a. As expected, the numerical operation of taking the frequency derivative degrades the signal-to-noise ratio somewhat. This degradation is more severe toward the low-frequency end of the scan, although the high-frequency end of the scan is not without its own problem—the interference due to parasitic system
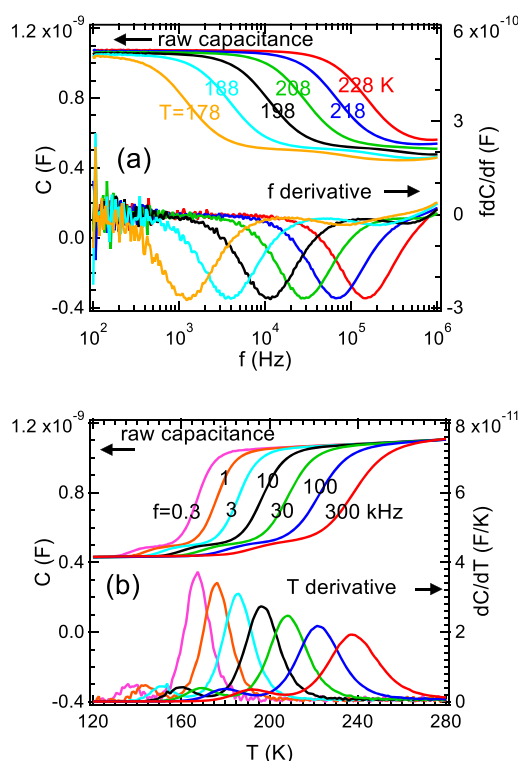

Figure 1. (a) Isothermal scans of raw capacitance versus frequency spectra (top) and frequency derivative capacitance fdC/df spectra (bottom) measured at various temperatures and (b) the isorate scans of raw capacitance versus temperature spectra (top) and temperature derivative capacitance dC/dT spectra (bottom) measured at various rates. The fdC/df and dC/dT derivative spectra exhibit peaks where the raw capacitance spectra exhibit step transitions, which are indicative of the electronic transition due to defects.

components such as the cable inductance and resistance may lead to resonance and even negative capacitance.

Two peaks are identifiable in Figure 1a, each indicative of the presence of one defect. In this work, we focus on the defect with a larger density, i.e., a larger fdC/df amplitude or a larger capacitance transition step. Figure 1b shows the raw capacitance versus temperature spectra and the isorate temperature derivative scans carried out at several rates, which also exhibit peaks that provide a signature of the same defects seen in the isothermal scans. The Arrhenius plot of the peaks observed in the isorate temperature derivative capacitance spectra is measured at various frequencies and shown in Figure 2 (circles). As expected from the conventional admittance spectroscopy practice, the data resemble a line. Next, we use line fitting (Figure 2, line) to extract the activation energy E_a of the defect from the slope of the line and the natural logarithmic attempt-to-escape frequency $\ln(\nu_0)$ from the intercept with the ordinate, which are 335 ± 1 meV and 30.8 ± 0.1 s^{-1}, respectively. As expected, the extractions of E_a and ν_0 from the isorate scans agree with those using the isothermal scans (data not shown).

RESULTS

Isothermal scans, which refer to scans that vary the rate ν while keeping the temperature T constant, are traditionally preferred by the admittance spectroscopy apparatus. Repeating isothermal scans at various temperatures leads to admittance spectroscopy data obtained in a two-dimensional temperature–rate space, as shown in Figure 3 in the form of a capacitance surface plot
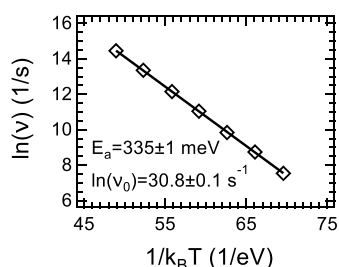
Figure 2. The Arrhenius plot constructed from the positions of the larger peak of the two peaks in each spectrum (symbols) observed in the isorate dC/dT spectra in Figure 1b and the line fitting (line) are used to extract the defect activation energy E_a = 335 ± 1 meV. The corresponding natural logarithmic attempt-to-escape frequency is $\ln(\nu_0)$ = 30.8 ± 0.1 s^{-1}.
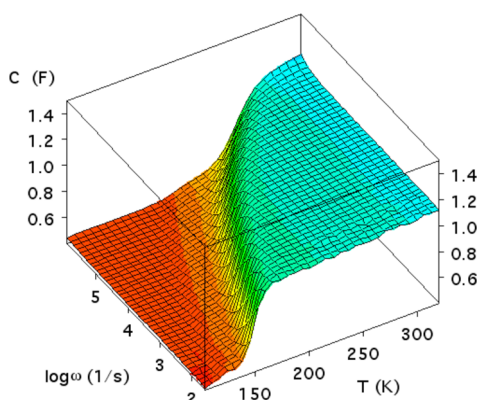

Figure 3. The surface plot of the raw capacitance signal $C(T, \nu)$ is displayed against the temperature−rate plane. The defect-induced capacitance transition produces the waterfall feature in the temperature−frequency plane. Information contained in the edge locus of the waterfall is used, after frequency or temperature differentiation, to construct the Arrhenius plot and extract E_a and ν_0 by the APL method. The isothermal and isorate scans at any (T_{fix}, ν_{fix}) point, with examples shown in Figure 1, may be visualized as "slicing" through the $C(T, \nu)$ surface in the 2D temperature−rate space.

displayed in the two-dimensional $T−\nu$ plane. The defect-induced capacitance transition produces the waterfall feature in the temperature−frequency plane. Information contained in the edge locus of the waterfall is used after frequency or temperature differentiation to construct the Arrhenius plot to produce $\nu(T)$—retrieving one-dimensional information that is only a subset of that contained in the original two-dimensional $C(T, \nu)$ surface—and extract E_a and ν_0 by the APL method. The mutually orthogonal isothermal and isorate scans at any (T_{fix}, ν_{fix}) point, with examples shown in Figure 1, may be visualized as "slicing" through the $C(T, \nu)$ surface in the 2D space.

We develop the Arrhenius transformation and matching method to overcome the one-dimensional Arrhenius plot limit by the classical APL method and circumvent the need to carry out the frequency/temperature derivative. Instead of simply using the peak positions taken from the frequency/temperature derivative spectra, the ATM method simultaneously exploits the mutually orthogonal isothermal and isorate admittance scans illustrated in Figure 3. The ATM method thus takes full utilization of the information contained in the entire two-dimensional temperature−rate space as opposed to the APL method, which relies on the one-dimensional information contained in the locus of the peak position of the frequency/

temperature derivative spectra (i.e., the waterfall edge of the $C(T, \nu)$ surface in Figure 3). Specifically, the temperature−rate transformation method exploits the second moment of the admittance (e.g., the curvature of the surface) in the $T−\nu$ space by simultaneously matching the isothermal and isorate scans at any (ν_{fix}, T_{fix}) point (example shown by thin dashed lines in Figure 3) according to the temperature−rate duality.

The temperature−rate duality was first realized by Agarwal et al. in DLTS.[13] Note that the two experimental parameters of ν and T in eq 1 are independently controllable. Because ν and T are related by eq 1 in the same thermal activation process defined by the same E_a and ν_0, a scan in the ν-space corresponds to an equivalent scan in the T-space, and vice versa. Consequently, scanning either ν or T while keeping the other constant leads to variations in capacitance that contain identical information. In this work, we extend Agarwal et al.'s concept of temperature−rate duality and use the Arrhenius equation (eq 1) as the foundation of a suite of Arrhenius transformations between the two experimentally controllable parameters (the temperature T and the rate ν) using the two parameters to be extracted (the activation energy E_a and the attempt-to-escape frequency ν_0).

We define two transformations derived from eq 1: the $T−E_a$ transformation

$$E_{a,T} = k_B T \ln(\nu_0/\nu_{fix}) \tag{2}$$

and the $\nu−E_a$ transformation

$$E_{a,\nu} = k_B T_{fix} \ln(\nu_0/\nu) \tag{3}$$

In eqs 2 and 3, T and ν are experimentally controlled variables. ν_0 is the free variable, whose use as a fitting parameter is explained next. Consider the two independent scans obtained through separate experiments: (i) the isorate scan $C(T)$ as T is scanned with $\nu = \nu_{fix}$ fixed and (ii) the isothermal scan $C(\nu)$ as ν is scanned with $T = T_{fix}$ fixed (e.g., indicated by dashed lines in Figure 3). We then can use the $T−E_a$ transformation in eq 2 to transform from T to $E_{a,T}$ and obtain a corresponding virtual scan $C(E_{a,T})$ in the activation energy space. For an experimentally obtained isothermal scan $C(\nu)$ in the ν-space, we use the $\nu−E_a$ transformation (eq 3) to transform from ν to $E_{a,\nu}$ and obtain a corresponding virtual scan $C(E_{a,\nu})$ also in the activation energy space. Note that the $T−E_a$ and $\nu−E_a$ transformations both share the same fitting parameter ν_0, whose value adjusts the curvatures of $C(E_{a,T})$ and $C(E_{a,\nu})$ simultaneously. The two experimental scans $C(\nu)$ and $C(T)$ probe the electronic response of the same thermally activation process. Therefore, the virtual scan $C(E_{a,\nu})$ transformed from $C(\nu)$ and the virtual scan $C(E_{a,T})$ transformed from the isorate scan $C(T)$ should agree with each other, if and only if the $T−E_a$ and $\nu−E_a$ transformations use the ν_0 value true to the thermal activation process physically responsible to both scans—this is the basis for the extraction of ν_0. Once ν_0 is determined according to the above fitting procedure, E_a is computed by eq 1 since E_a and ν_0 together satisfy eq 1 (T_{fix}, ν_{fix}). Note that the above procedure does not depend on identifying peak features, such as those in the fdC/df spectra; hence, no numerical derivative is required.

We call the above procedure the activation energy projection variation of the ATM method because both T and ν are transformed to E_a, so the scans are projected to the activation energy space. We apply the new method to our case study for electronic transitions in GaAsN. We transformed the experimental isothermal scan $C(\nu)$ taken at 197 K (Figure 1b) using

$T-E_a$ transformation to obtain the isothermal scan $C(E_{a,\nu})$ in the activation energy space (Figure 4, solid line). Figure 4 also shows
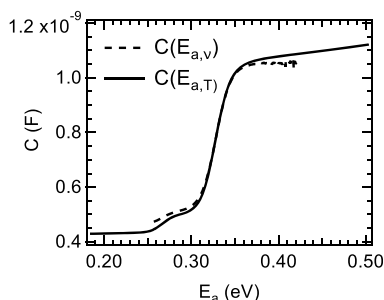

Figure 4. The isothermal scan $C(E_{a,\nu})$ (solid line) and isorate scan $C(E_{a,T})$ (dashed line) are transformed and matched using $\log_{10}(\nu_0) = 13.1$ s^{-1} as the best-fit transformation parameter. The raw isothermal and isorate scans are taken at $T_{fix} = 197$ K and $\nu_{fix} = 10$ kHz, respectively (dashed lines in Figure 3). The activation energy $E_a = 338$ meV is calculated using the best-fit ν_0 value from eq 1 at the (T_{fix}, ν_{fix}) point.

the isorate scan $C(E_{a,T})$ in the activation energy space (dashed line) transformed from the experimental isorate scan $C(T)$ (Figure 1a) taken at 10 kHz using the $\nu-E_a$ transformation. The same value of $\log_{10}\nu_0 = 13.1$ 1/s is used in both the $T-E_a$ and $\nu-E_a$ transformations, i.e., eqs 2 and 3, respectively. An activation energy of $E_a = 338$ meV is calculated using eq 1 ($\log_{10}\nu_0 = 13.1$ 1/s) at (T_{fix}, ν_{fix}).

Above, we use the $T-E_a$ and $\nu-E_a$ transformations, i.e., eqs 2 and 3, to project the experimental isothermal and isorate scans onto the activation energy space. These two transformations both rely on ν_0 as the free-tuning variable that functions as the fitting parameter to adjust and match the projected isothermal and isorate scans in the activation energy space. E_a is lastly calculated from ν_0 after the best matching/fitting is determined. We can construct an alternative variation of the AEP method by exploiting the $E_a-\nu_0$ symmetry in eq 1. Similar to $T-E_a$ and $\nu-E_a$ transformations, we introduce the $T-\nu_0$ transformation

$$\nu_0 = \nu_{fix} \exp(E_a/k_B T) \tag{4}$$

and the $\nu-\nu_0$ transformation

$$\nu_0 = \nu \exp(E_a/k_B T_{fix}) \tag{5}$$

In these two transformations, T and ν are experimentally controlled variables, but E_a is the free-tuning variable. One then uses E_a as the fitting parameter to project the experimental isothermal and isorate scans onto the attempt-to-escape frequency space. Matching these projected isothermal and isorate scans in the attempt-to-escape frequency space determines the best choice of E_a, from which ν_0 is calculated according to eq 1 at (T_{fix}, ν_{fix}), or reads from the common peak shared by transformed isothermal and isorate scans in the attempt-to-escape frequency space.

The next variation of the ATM method is based on direct transformation between T and ν.[14] Rearranging the expression produced by equating the right-hand sides of eqs 2 and 3, we arrive at

$$T = T_{fix} \times (\ln \nu_0 - \ln \nu)/(\ln \nu_0 - \ln \nu_{fix}) \tag{6}$$

which we call the $\nu-T$ transformation. We use the $\nu-T$ transformation in eq 6 to transform from ν to T and obtain a corresponding virtual scan $C(T_\nu)$ from an experimental isothermal scan $C(\nu)$. Note that the $T-\nu$ transformation in eq

6 depends on both ν_0 and E_a, but only one of them (for example, E_a) will be used as the fitting parameter to adjust the curvatures of $C(T_\nu)$ because they are related by eq 1 at (T_{fix}, ν_{fix}). The two experimental scans $C(\nu)$ and $C(T)$ probe the electronic response of the same thermally activation process. Therefore, the virtual scan $C(T_\nu)$ transformed from $C(\nu)$ and the experimental isorate scan $C(T)$ should agree with each other, if and only if the $\nu-T$ transformation uses the E_a value true to the thermal activation process physically responsible to both scans—this is the basis for the extraction of E_a. Once E_a is determined according to the above fitting procedure, ν_0 is computed by eq 1. An example of the $\nu-T$ transformation variation of the ATM method is demonstrated in its application to the study of electronic transitions in GaAsN, as shown in Figure 5. We transformed one experimental isothermal scan
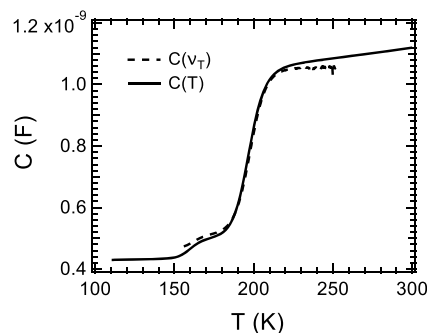

Figure 5. The $C(T_\nu)$ scan (dashed line), $T-\nu$ transformed from the original isothermal scan $C(\nu)$, matches the experimental isorate scan $C(T)$ (solid line using $\log_{10}(\nu_0) = 13.1$ s^{-1} as the best fitting transformation parameter in eq 6. The raw scans are taken at $T_{fix} = 197$ K and $\nu_{fix} = 10$ kHz, respectively (dashed lines in Figure 3). The activation energy of $E_a = 338$ meV is calculated using the best-fit ν_0 value from eq 1 at the (T_{fix}, ν_{fix}) point.

$C(\nu)$ taken at 197 K (Figure 1b) using the $\nu-T$ transformation (eq 6) to obtain the virtual scan $C(T_\nu)$. Figure 5 also shows the experimental isorate scan $C(T)$ taken at 10 kHz. When a value of $\log_{10}\nu_0 = 13.1$ 1/s is used in $\nu-T$ transformations, $C(T_\nu)$ agrees well with $C(T)$. Next, the E_a of 338 meV is calculated from ν_0 by eq 1 at (T_{fix}, ν_{fix}).

Situations may arise where only one kind of scan, either isorate or isothermal, is available while the other kind is either unavailable or sparsely distributed in the $T-\nu$ space. Then, it is not practical to implement the variations of $\nu-T$ transformation, the activation energy project, or the attempt-to-escape projection described above, which all rely on simultaneous utilization of isorate and isothermal scans. In this case, we can use one of eqs 2−5 to project all scans of that particular kind, isorate or isothermal, to either the activation energy space or the attempt-to-escape frequency space. Figure 6 shows an example of projecting all the isorate $C(\nu)$ scans (taken from Figure 1b) onto the activation energy space using only the $T-E_a$ transformation (eq 2). The resultant $C(E_{a,T})$ all collapse on top of one another, manifesting that the same defect, discrete or extended, is the underlying root to the admittance response in the two-dimensional $T-\nu$ space. Moreover, the notion that all the $C(E_{a,T})$ spectra collapse on each other is in fact a condition of best fitting for extracting ν_0 used in eq 2, hence the reason to call this procedure the activation energy collapsing method.

To take full advantage of the symmetry between T and ν, another ATM variation can be implemented with the $T-\nu$
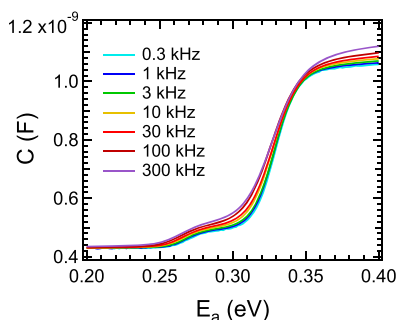
Figure 6. All the isorate $C(T)$ scans from Figure 1a are projected onto the activation energy space using only the $T−E_a$ transformation (eq 2) with E_a = 338 meV. The resultant $C(E_{a,T})$ spectra all collapse on top of one another, which is the condition of best fitting for extracting E_a used in eq 2, hence the reason to call this procedure the activation energy collapsing method.

variation of Arrhenius transformation to transform T to ν, producing the transformed $C(\nu_T)$ from the experimental isorate scan $C(T)$, and matched to the experimental isothermal $C(\nu)$ scan. The $T−\nu$ transformation is derived by rearranging the expression produced by equating the right-hand sides of eqs 4 and 5

$$\nu = \nu_{\text{fix}} \times \exp[E_a/k_B \times (T^{-1} - T_{\text{fix}}^{-1})] \tag{7}$$

One can use the $T−\nu$ transformation to transform from T to ν and obtain a corresponding virtual scan $C(\nu_T)$ from an experimental isorate scan $C(T)$. The best-fit E_a value used in eq 7 results in $C(\nu_T)$ matching the experimental isothermal scan $C(\nu)$. Once E_a is determined according to the above fitting procedure, ν_0 is computed by eq 1 at $(T_{\text{fix}}, \nu_{\text{fix}})$.

■ DISCUSSION

We used the imaginary part of admittance, i.e., the capacitance, in the narrative and calculation in the preceding text, although it is understood that identical information can be retrieved from the real part of admittance, i.e., the conductance.[1] Figure 7 shows the surface plot of the raw conductance signal $G/\omega(T, \nu)$ displayed against the temperature−frequency plane. To observe a defect-induced peak feature similar to the frequency derivative capacitance spectra, the conductance is divided by the angular velocity ω to arrive at G/ω. The isothermal and isorate scans at any $(T_{\text{fix}}, \nu_{\text{fix}})$ point may be visualized as "slicing" through the $G/\omega(T, \nu)$ surface in the 2D temperature−rate space.

Figure 7. The surface plot of the raw conductance signal $G/\omega(T, \nu)$ is displayed against the temperature−rate plane. Information contained in the locus of the defect-induced conductance peak could be used to construct the Arrhenius plot and extract E_a and ν_0 by the APL method. The isothermal and isorate scans at any $(T_{\text{fix}}, \nu_{\text{fix}})$ point may be visualized as "slicing" through the $G/\omega(T, \nu)$ surface in the 2D temperature−rate space.
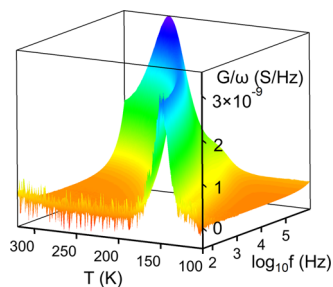
$\omega(T, \nu)$ surface in the 2D space. Figure 8 shows that one example of the $G/\omega(T_\nu)$ scan (dashed line), $T−\nu$ transformed
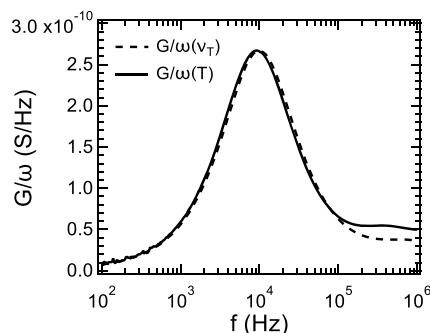

Figure 8. The $G/\omega(T_\nu)$ scan (dashed line), $T−\nu$ transformed from the original isorate scan $G/\omega(T)$, matches the experimental isothermal scan $G/\omega(\nu)$ (solid line) using E_a = 338 meV as the best fitting transformation parameter in eq 7. The raw scans are taken at T_{fix} = 197 K and ν_{fix} = 10 kHz, respectively (dashed lines in Figure 3). The activation energy of $\log_{10}(\nu_0)$ = 13.1 s^{-1} is calculated using the best-fit E_a value from eq 1 at the $(T_{\text{fix}}, \nu_{\text{fix}})$ point.

from the original isorate scan $G/\omega(T)$, matches the experimental isothermal scan $G/\omega(\nu)$ (solid line) using E_a = 338 meV as the best fitting transformation parameter in eq 7. The raw scans are taken at T_{fix} = 197 K and ν_{fix} = 10 kHz, respectively (dashed lines in Figure 3). The activation energy of $\log_{10}(\nu_0)$ = 13.1 s^{-1} is calculated using the best-fit E_a value from eq 1 at the $(T_{\text{fix}}, \nu_{\text{fix}})$ point.

We note that the underlying assumption of line fitting for the Arrhenius plot, yielding a single value of E_a and ν_0 in the classical APL method,[15] is for them to be invariant over the entire two-dimensional $T−\nu$ space scanned in the experiment. In contrast, when the data fitting is confined to a small range near T_{fix} and ν_{fix} (e.g., ~±10 K in Figure 4), then the activation energy project method extracts E_a and ν_0 that are local to that $(T_{\text{fix}}, \nu_{\text{fix}})$ point. The ATM method thus reveals details of the temperature-dependent behavior of E_a and ν_0 that is not possible by the classic APL methods because the physical information contained in $C(T, \nu)$, a 2D array of size $N \times M$ (N and M are the number of T and ν data points, respectively), is more than sufficient for solving two independent size-N 1D arrays $E_a(T)$ and $\nu_0(T)$. Specifically, the four variations of ATM that requires transformation and matching between one $C(\nu)$ spectrum and one $C(T)$ spectrum—the activation energy projection, the attempt-to-escape frequency projection, the $T−\nu$ transformation, and the $\nu−T$ transformation—are capable of extracting E_a and ν_0 local to $(T_{\text{fix}}, \nu_{\text{fix}})$, which may be temperature-dependent. The two collapse variations onto the activation energy and the attempt-to-escape frequency space respectively extract E_a and ν_0 that are global to the entire temperature range, similar to APL, and are temperature-independent.

The numerical differentiation operation, whether with respect to frequency or temperature, may significantly degrade the signal-to-noise ratio of the derivative capacitance spectra. In extreme situations (see Figure S1,Supporting Information, the derivative spectra can barely reveal the presence of a defect signature (peak), but the accurate extraction of peak positions in these spectra is a difficult task, rendering the conventional APL method of plotting the Arrhenius plot and extraction of E_a and ν_0 plainly unreliable if not impossible. The raw admittance data prior to the numerical differentiation step do not suffer the said

degradation of the signal-to-noise ratio. Because the ATM method directly uses the raw capacitance or conductance data, it is more likely to achieve a reliable extraction of ν_0 and E_a (see Figure S2, Supporting Information), even when the conventional APL method fails.

CONCLUSIONS

In conclusion, we have developed an admittance spectroscopy characterization method to extract the activation energy E_a and the pre-exponential factor ν_0 of the thermally activated process without using the Arrhenius plot and without taking the frequency or temperature derivative (see Figure S3 for a diagram comparing the processing steps of the ATM method to those of the APL method). This method is developed upon the fundamental temperature—rate duality relationship based on the Arrhenius equation and extracts E_a and ν_0 by transforming the experimental isothermal and isorate scans of raw capacitance or conductance onto one of the four virtual spaces—activation energy, attempt-to-escape frequency, temperature, and rate— and matching the resultant virtual scans. The extraction can be done at any temperature point and therefore is able to unambiguously solve E_a, ν_0, and their temperature dependence.

ASSOCIATED CONTENT

Ⓢ Supporting Information

The Supporting Information is available free of charge at https://pubs.acs.org/doi/10.1021/acs.jpcc.0c10853.

> Additional information on admittance spectroscopy data with relatively poor signal-to-noise ratio (Figure S1) and the ATM method's stronger tolerance (Figure S2); one diagram (Figure S3) comparing the typical processing steps of the conventional APL method and the ATM method (PDF)

AUTHOR INFORMATION

Corresponding Author

Jian V. Li − *Department of Aeronautics and Astronautics, National Cheng Kung University, Tainan 70101, Taiwan;* ⓘ orcid.org/0000-0003-3623-3044; Phone: 886-06-2757575; Email: jianvli@mail.ncku.edu.tw

Complete contact information is available at:
https://pubs.acs.org/10.1021/acs.jpcc.0c10853

Notes

The author declares no competing financial interest.

ACKNOWLEDGMENTS

REFERENCES

(1) Losee, D. L. Admittance spectroscopy of impurity levels in Schottky barriers. *J. Appl. Phys.* **1975**, *46*, 2204−2214.

(2) Walter, T.; Herberholz, R.; Müller, C.; Schock, H. W. Determination of defect distributions from admittance measurements and application to Cu(In,Ga)Se$_2$ based heterojunctions. *J. Appl. Phys.* **1996**, *80*, 4411−4420.

(3) Blood, P.; Orton, J. W. *The Electrical Characterization of Semiconductors: Majority Carriers and Electron States*; Academic Press: London, U.K., 1992.

(4) Li, J. V.; Johnston, S. W.; Li, X.; Albin, D. S.; Gessert, T. A.; Levi, D. H. Discussion of some "trap signatures" observed by admittance spectroscopy in CdTe thin-film solar cells. *J. Appl. Phys.* **2010**, *108*, No. 064501.

(5) Sah, C. T. *Fundamentals of Solid-State Electronics*; World Press: Singapore, 1990.

(6) Arrhenius, S. On the reaction rate of the inversion of non-refined sugar upon souring. *Z. Phys. Chem.* **1889**, *4*, 226−248.

(7) Cavicchi, R. E.; Lang, D. V.; Gershoni, D.; Sergent, A. M.; Vandenberg, J. M.; Chu, S. N. G.; Panish, M. B. Admittance spectroscopy measurement of band offsets in strained layers of In$_x$Ga$_{1−x}$As grown on InP. *Appl. Phys. Lett.* **1989**, *54*, 739−741.

(8) Li, J. V.; Levi, D. H. Determining the defect density of states by temperature derivative admittance spectroscopy. *J. Appl. Phys.* **2011**, *109*, No. 083701.

(9) Van Vechten, J. A.; Thurmond, C. D. Entropy of ionization and temperature variation of ionization levels of defects in semiconductors. *Phys. Rev. B* **1976**, *14*, 3539−3550.

(10) Wickramaratne, D.; Dreyer, C. E.; Monserrat, B.; Shen, J.-X.; Lyons, J. L.; Alkauskas, A.; Van de Walle, C. G. Defect identification based on first-principles calculations for deep level transient spectroscopy. *Appl. Phys. Lett.* **2018**, *113*, 192106.

(11) *Capacitance Spectroscopy of Semiconductors*; Li, J. V., Ferrari, G., Eds.; Pan Stanford Publishing: Singapore, 2018.

(12) Johnston, S. W.; Kurtz, S. R. Comparison of a dominant electron trap in *n*-type and *p*-type GaNAs using deep-level transient spectroscopy. *J. Vac. Sci. Technol., A* **2006**, *24*, 1252−1257.

(13) Agarwal, S.; Mohapatra, Y. N.; Singh, V. A. Temperature − time duality and deep level spectroscopies. *J. Appl. Phys.* **1995**, *77*, 3155−3161.

(14) Li, J. V.; Johnston, S. W.; Yan, Y.; Levi, D. H. Measuring temperature-dependent activation energy in thermally activated processes: A 2D Arrhenius plot method. *Rev. Sci. Instrum.* **2010**, *81*, No. 033910.

(15) Wang, S.; Kaienburg, P.; Klingebiel, B.; Schillings, D.; Kirchartz, T. Understanding thermal admittance spectroscopy in low-mobility semiconductors. *J. Phys. Chem. C* **2018**, *122*, 9795−9803.

Supporting information for

Defect Characterization Using Raw Admittance Spectroscopy

Jian V. Li[*]

Department of Aeronautics and Astronautics, National Cheng Kung University

1 University Road, Tainan, 70101 Taiwan

Corresponding author:
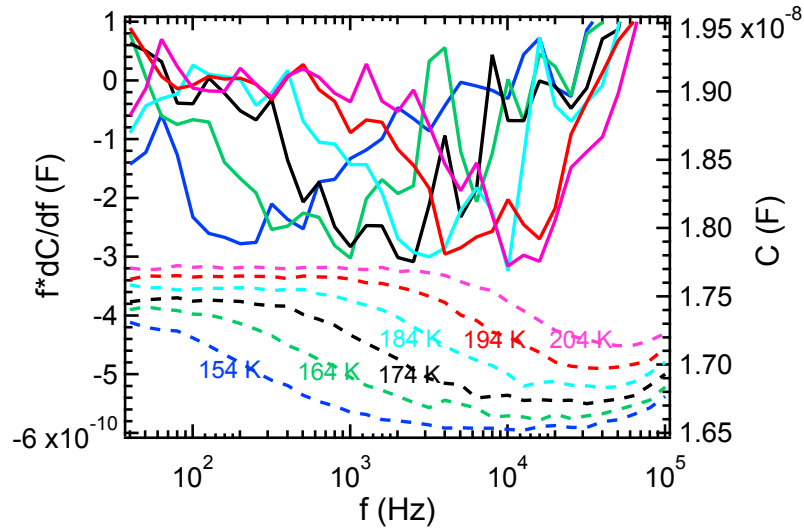
Email: jianvli@ncku.edu.tw

Figure S1. This figure shows the raw capacitance-frequency spectra (dashed lines) measured from a GaAs solar cell device grown by hydride vapor phase epitaxy at several temperatures and the corresponding frequency derivative f*dC/df spectra thereof (solid lines, using the same coloring scheme as the C-f spectra). Due to the numerical differentiation, the f*dC/df spectra exhibit quite poor signal-to-noise ratios and can barely reveal a defect signature (negative peak). Extracting peak positions in these spectra is a difficult task. Consequently, the conventional APL method of plotting the Arrhenius plot and extracting E_a and ν_0 is unreliable if not impossible.
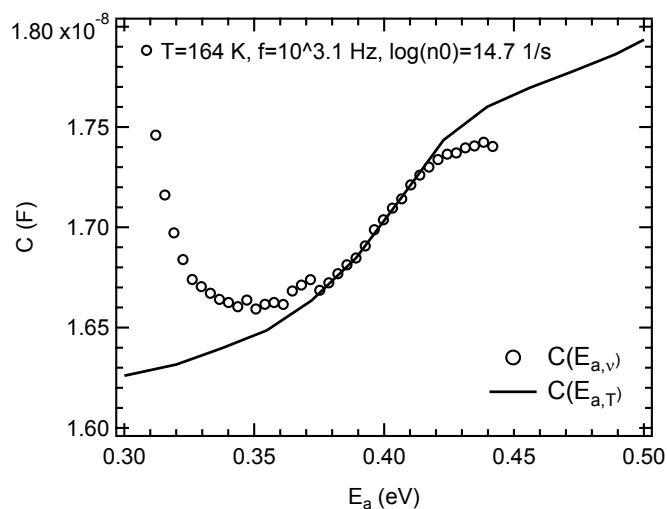
Figure S2. Figure S2 shows the application of the activation energy projection variation of the ATM method to transform and match the iso-thermal (symbols) and iso-rate (line) scans using data shown in Figure S1. The new ATM method described in this work directly uses the capacitance (i.e., the raw admittance data), which do not suffer the degradation of signal-to-noise ratio due to the numerical differentiation. The ATM method is able to achieve a good agreement between $C(E_{a,v})$ and $C(E_{a,T})$ for a reliable extraction of $\log_{10}(v_0)$=14.7 1/s and E_a=0.378 eV per Eq (1) at the fixed temperature and rate of 164 K and 1259 Hz, respectively.

Raw C(f) spectra at various T

Conventional APL method (Figs. 1&2)

The Ea collapsing ATM method (Fig. 6)

Numerical differentiation to produce f*dC/df spectra

Reconstruct to obtain C(T) spectra at various f

Transform f to $E_{a,v}$ using v_0 in Eq. 3

(optional) Curve fitting the f*dC/df spectra

Transform T to $E_{a,T}$ and f to $E_{a,v}$ using v_0 in Eqs. 2&3

Match all $C(E_{a,v})$ spectra to obtain best fit value of v_0

Identify peaks in f*dC/df spectra

Match $C(E_{a,T})$ and $C(E_{a,v})$ to obtain best fit value of v_0

Calculate Ea from Eq. 1 using the above v_0

Use the peak data to construct Arrhenius plot

Calculate Ea from Eq. 1 using the above v_0

Line-fitting the Arrhenius plot to extract E_a and v_0
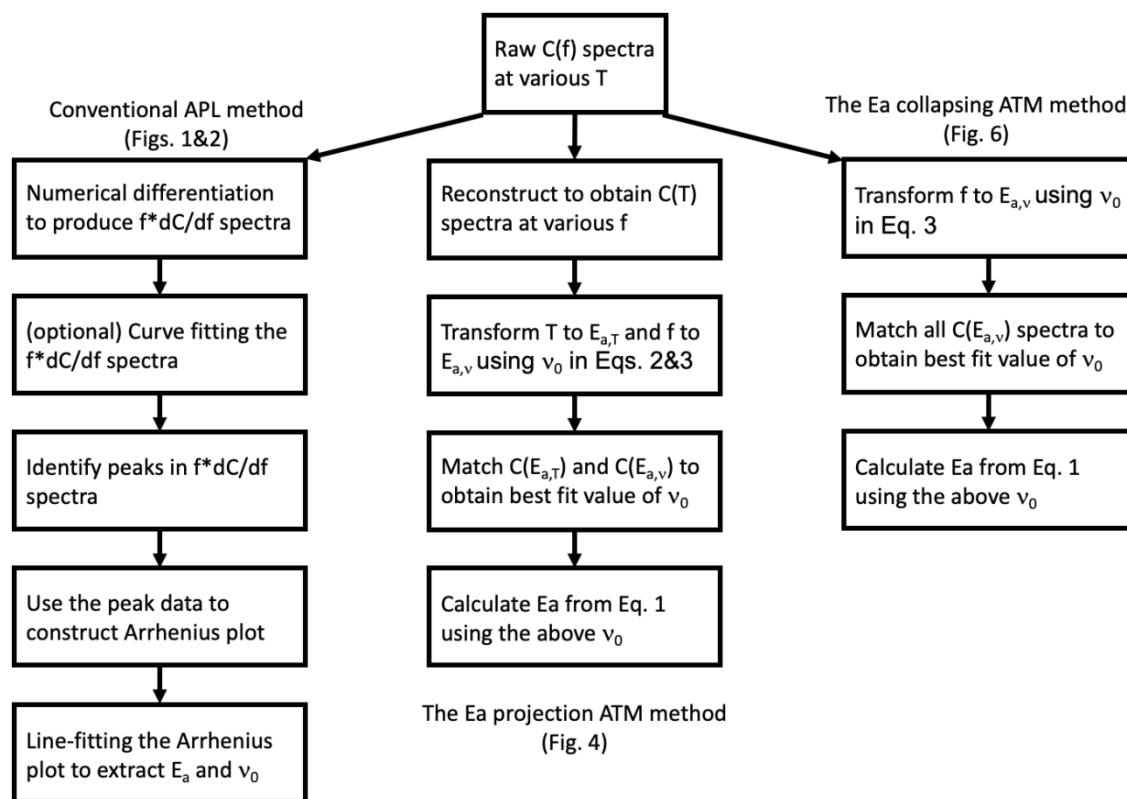
The Ea projection ATM method (Fig. 4)

Figure S3. A diagram comparing the processing steps of the APL method (left column) and two variations (middle and right columns) of the ATM method. The ATM method takes a radically different approach to extract E_a and v_0, possibly with fewer steps. Because of the reduced processing complexity (no numerical differentiation) and steps, the ATM method may save computing and analysis time compared to the conventional APL method